Scripta Materialia 176 (2020) 78–82

Contents lists available at ScienceDirect

Scripta Materialia

journal homepage: www.elsevier.com/locate/scriptamat

Reactive flash sintering of the complex oxide $Li_{0.5}La_{0.5}TiO_3$ starting from an amorphous precursor powder

Viviana Avila[a], Bola Yoon[a], Rubens R. Ingraci Neto[a], Ronaldo S. Silva[b], Sanjit Ghose[c], Rishi Raj[a], Lílian M. Jesus[a,d,1,*]

[a] Materials Science and Engineering Program, Department of Mechanical Engineering, University of Colorado at Boulder (UCB), Boulder, CO 80309-0427, USA
[b] Group of Functional Nanomaterials, Department of Physics, Federal University of Sergipe, São Cristóvão, SE 49100-000, Brazil
[c] Brookhaven National Laboratory, National Synchrotron Light Source II, Upton, NY 11973-5000, USA
[d] Group of Advanced Functional Materials, Department of Physics, Federal University of São Carlos (UFSCar), São Carlos, SP 13565-905, Brazil

ARTICLE INFO

Article history:
Received 14 August 2019
Revised 9 September 2019
Accepted 24 September 2019

Keywords:
Reactive flash
Powder processing
X-ray diffraction (XRD)
Synchrotron radiation
Electrical properties

ABSTRACT

We report the transformation of an amorphous mixture of $Li_{0.5}La_{0.5}TiO_3$ (LLTO) directly into a single phase dense polycrystal, all within a few seconds at about 800 °C by the flash method. The starting material is a chemically-prepared precursor powder that experiences concurrent crystallization and densification to cubic LLTO during the flash event, as shown by *in-situ* X-ray measurements. The experiments were conducted at a constant heating rate with fields from 80 to 120 V cm^{-1} and a current limit of 60 mA mm^{-2}. The resulting polycrystal yielded a bulk conductivity of 0.5 mS cm^{-1}.

The application of flash-sintering has recently expanded into "reactive flash sintering" where commercially available powders of constituent oxides are mixed and flashed, with the unusual result that a dense polycrystal is obtained directly from these elemental powders [1–5]. The reaction between crystalline powders of bismuth and iron oxides produced single phase bismuth ferrite in a matter of seconds under flash [6]. Reactive flash of a four component material was recently reported, where alumina doped lithium lanthanum zirconate was obtained, again, from commercial oxide powders [7]. Beyond the production of ceramics from the mixture of elemental oxides, the use of an electric field has also been combined with a chemical synthesis method to produce $CaCu_3Ti_4O_{12}$ (CCTO) perovskite [8,9]. In this case, the amorphous precursor powder first crystallized into intermediate phases that later reacted to form CCTO, then sintering was achieved at higher temperature as a result of the flash [8].

$Li_{0.5}La_{0.5}TiO_3$ (LLTO) has been extensively studied due to its ionic conductivity and hence its potential as a solid electrolyte in electrochemical devices [10–13]. Recently, it has also been proposed as a catalyst for the polysulfide conversion reaction [14] and as a coating material to improve cathode performance [15]. The structural characteristics in compounds of the form $Li_{2/3-x}Li_{3x}TiO_3$ depend crucially on the thermal treatment and the Li content of the oxides [11,16]. Structures including cubic, hexagonal, tetragonal, and orthorhombic perovskite-type unit cells have been identified for this system [17,18]. In the conventional ceramic method, production of single-phased highly dense LLTO involves two different steps, synthesis (at $T > 1000$ °C) and sintering (usually at $T = 1350$ °C), comprising several hours and high temperatures [16,19,20]. Additionally, thermal quenching is required in order to stabilize the cubic phase, which has a higher ionic conductivity [16,21].

In the present work, a highly reactive LLTO amorphous powder was prepared by the polymeric precursor route and directly flash processed under different electric field strengths. This is the first report of a near fully-dense Li-conductor material produced by the reactive flash method, made possible due to the combination of a chemical synthesis route and field-assisted processing, which accelerates crystallization and sintering rates.

The polymeric precursor was prepared using the following starting materials: Li_2CO_3 (Sigma Aldrich, 99%), $La(NO_3)_3{\cdot}6H_2O$ (Metaquimica, 99%), and $Ti[OCH(CH_3)_2]_4$ (Alfa Aesar, 97%). Stoichiometric amounts of the cationic precursors were mixed with citric acid (CA), previously dissolved in distilled water (0.1 g ml^{-1}),

* Corresponding author at: Materials Science and Engineering Program, Department of Mechanical Engineering, University of Colorado at Boulder (UCB), Boulder, CO 80309-0427, United States.
E-mail address: lilian@df.ufscar.br (L.M. Jesus).
[1] Permanent address: Group of Advanced Functional Materials, Department of Physics, Federal University of São Carlos (UFSCar), São Carlos, SP 13565-905, Brazil.

https://doi.org/10.1016/j.scriptamat.2019.09.037
1359-6462/

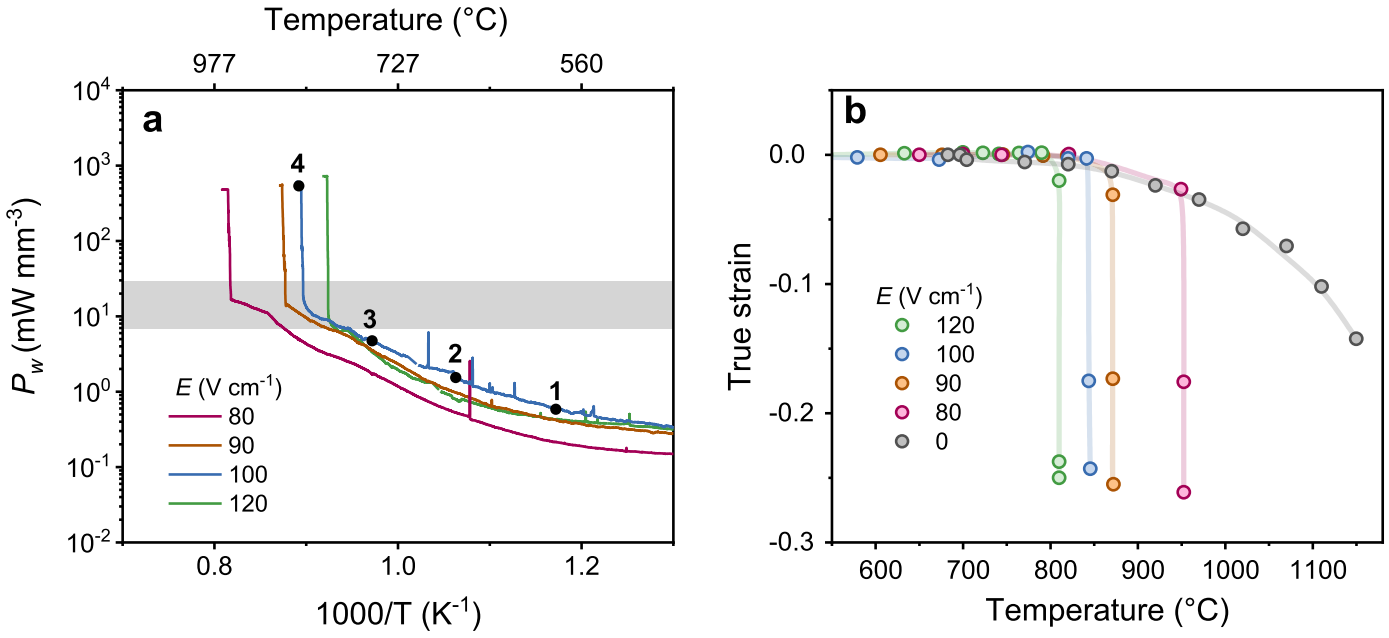

Fig. 1. (a) Arrhenius plot for the power dissipation P_w and (b) true linear strain as a function of furnace temperature, for samples processed at different field strengths. For all these experiments the current density limit was set as $J = 60$ mA mm^{-2}.

in the molar ratio of 1:3 (La/Li:CA) for lanthanum and lithium, and 1:6 (Ti:CA) for titanium. Ethylene glycol (EG) was then added to the citrates, in a mass ratio of 3:2 (CA:EG), in order to promote polymerization. The resulting polyesters were mixed, forming a transparent and yellowish (La,Li,Ti)-containing resin. This resin was heated to 120 °C to eliminate water excess, then annealed at 550 °C for 4 h with a heating rate of 2 °C min^{-1} to remove the organic compounds. The resulting LLTO precursor powder was white and amorphous. The powders were cold pressed with a uniaxial pressure of 275 MPa into a dog-bone shape with a gage length of 15.0 mm, width of 3.5 mm and a thickness of ~1.3 mm. These specimens were flash processed as described below.

The flash experiments were performed in a conventional furnace with the electric field supplied to the dog-bones via platinum wires. Platinum paste was applied to the ears of the dog-bone to improve electrical contact. The power was provided to the specimen by a KL 3000 W DC power supply (Glassman High Voltage, Inc., High Bridge, NJ). The current flowing across the specimens was recorded by a multimeter (Model 2000 Keithley Instruments, Cleveland, OH). The experiments were carried out in constant heating rate mode. In this method, the electric field is applied, and the furnace is heated at a constant rate (10 °C min^{-1}) until the onset of the flash is signaled by an abrupt increase in conductivity. Then the power supply is switched to current control with a pre-set current limit (60 mA mm^{-2}). This current density was held for 45 s, after which the power to the specimen and to the furnace was turned off.

The results from the flash experiments are given in Fig. 1. The Arrhenius plots of the power density P_w at field strengths of 80, 90, 100, and 120 V cm^{-1} are shown in Fig. 1a. P_w displays a sharp increase that signals the onset of flash. The inflexion in the power density curves lies in the 7–30 mW mm^{-3} range, consistent with the phenomenological discovery that nearly all ceramics flash in this range of power density regardless of field, temperature or composition [22].

The shrinkage curves in Fig. 1b show sudden sintering at the onset of flash. The density of these specimens was determined via Archimedes method and found to be from 96 to 98%. For the sake of comparison with conventional processing, a dog-bone specimen was sintered (without electric field) in the same furnace at 10 °C min^{-1} up to 1150 °C, when the furnace was turned off. The density of this specimen was only 78%. Despite the formation of the perovskite LLTO phase, a highly porous microstructure was obtained, as shown in the micrograph and X-ray diffraction (XRD) pattern presented in the Supplementary Material Figure S1.

Phase development during flash processing was investigated through *in-situ* XRD. These experiments were carried out at the beamline XPD 28ID-2 of the National Synchrotron Light Source II (NSLS II) at Brookhaven National Laboratory, using a wavelength of 0.18203 Å (68.112 keV) [23,24]. The experimental setup is described in the Supplementary Material Figure S2. Time dependent XRD patterns showing crystallization and phase evolution of a specimen processed under 100 V cm^{-1} are presented in Video S1. As an illustration, representative patterns were extracted at points 1–4 indicated in Fig. 1a. These patterns are presented in Fig. 2a along with that for the precursor powder, which does not possess well-defined Bragg reflections indicating no long-range ordering. By increasing the temperature during the electric field-assisted processing, some small and broad peaks start to appear. However, the LLTO crystallization occurs essentially during the flash event, meaning that the amorphous precursor powder transforms into the single-phase cubic LLTO and densifies simultaneously. It has been established that, irrespective of the synthesis method used, the formation of LLTO is a multistage process [19,25]. Indeed, after calcining the precursor powder at 800 °C for 2 h without the application of an electric field we verified the formation of tetragonal-LLTO, Li_2TiO_3, and $La_4Ti_9O_{24}$ intermediate phases (Supplementary Material Figure S3). Only when this powder was heated to 1150 °C, the intermediate phases dissolved into the LLTO matrix, with residual superlattice reflections still detectable (Supplementary Material Figure S1b). Upon the application of the electric field, however, the amorphous powder was driven directly to cubic LLTO with no significant formation of intermediate phases or superlattice reflections. We can thus conclude that the flash method not only accelerates the cubic LLTO crystallization, but it also changes the reaction path by avoiding the formation of intermediate phases (*i.e.*, the electric field stimulates the nucleation process of cubic LLTO while hindering that of Li_2TiO_3

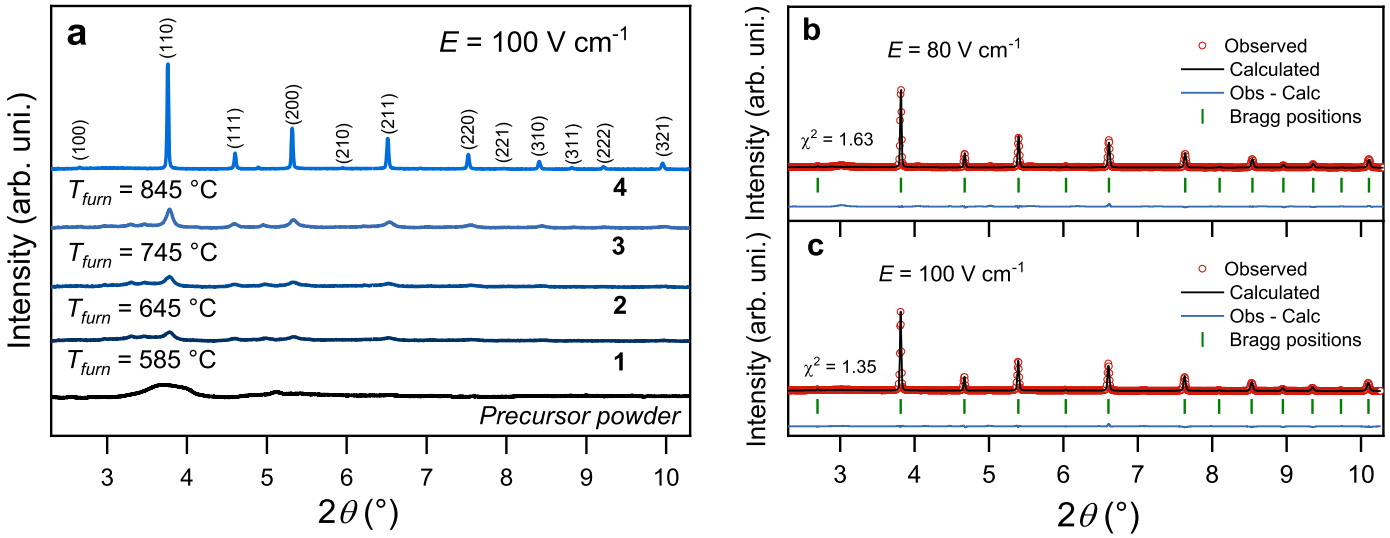

Fig. 2. (a) XRD patterns of the ceramic during processing under $E = 100\,V\ cm^{-1}$ at the representative instances 1 to 4, as indicated in Fig. 1a (T_{furn} stands for furnace temperature). (b)-(c) Rietveld analysis for the ceramics after reactive flash at $E = 80$ and $100\,V\ cm^{-1}$, respectively.

and $La_4Ti_9O_{24}$). This is consistent with the observation that the Gibbs free energy of phase transformation may be either reduced or enhanced by an electric field depending on the ratio of the dielectric constants of the old and new phases [26].

The XRD profiles of the final ceramics, measured at room temperature, for samples processed under $E = 80$ and $100\,V\ cm^{-1}$ are presented in Fig. 2b and c, respectively. The refined patterns obtained by Rietveld analysis, performed using FullProf software [27], are also included. These patterns were successfully refined considering a single cubic perovskite with space group $Pm\bar{3}m$, using the ICSD Card No. 76,180. The lattice constant a and goodness-of-fit χ^2 are $a = 3.866(1)$ Å, $\chi^2 = 1.63$, and $a = 3.869(1)$ Å, $\chi^2 = 1.35$, for $E = 80$ and $100\,V\ cm^{-1}$, respectively. It is known that the lattice parameter for the cubic form of the $Li_{2/3-x}Li_{3x}TiO_3$ system decreases with increasing x [28]. The values of a obtained here agree with those reported in previous studies for the cubic phase of the $Li_{3x}La_{2/3-x}TiO_3$ system with $x = 0.167$ [11,18,29]. Therefore, our samples retain a high Li content, close the nominal composition, and no significant long-range structural difference is observed for samples processed with different electric field strengths. It is worth mentioning that, for solid state synthesized $Li_{0.5}La_{0.5}TiO_3$, a tetragonal structure is usually achieved by slowly cooling the ceramics after sintering. Here, we attribute the stabilization of the cubic phase to the use of a chemical synthesis route combined with the flash method, implying high heating and cooling rates.

The microstructure was examined in two ways. In one case the ceramics were polished and thermally etched at 1050 °C for 10 min, while in the other case they were fractured as-sintered. The specimens were sputter coated with Pt and analyzed by scanning electron microscopy (SEM), using a SU3500 (Hitachi, Tokyo, Japan). The micrographs are given in Fig. 3, showing a uniform and dense microstructure, consistent with the density measurements. The average grain size (AGS) was evaluated by applying the standard intercept length method and is presented in Table 1. Note that the AGS of the specimen processed with $100\,V\ cm^{-1}$ is twice larger than that of the one processed with $80\,V\ cm^{-1}$. For flash sintering, the influence of field strength on grain size has been found to be variable and dependent on the material. For instance, TiO_2 showed an increase in AGS proportional to the electric field [30], while CCTO displayed the opposite behavior [8]. Here, the AGS of LLTO increased with E. The values of temperature reached by the ceramics during the flash were estimated by the black-body

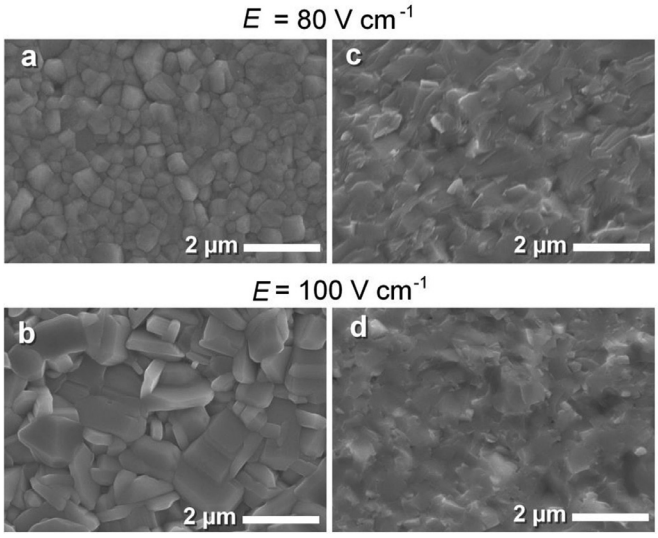

Fig. 3. Micrographs of (a)-(b) polished and thermally etched surfaces and of (c)-(d) fracture cross-sections of the as-sintered field assisted processed ceramics at 80 and $100\,V\ cm^{-1}$, as indicated.

Table 1
Electric field (E), average grain size (AGS), bulk (σ_{Bulk}) and grain boundary (σ_{GB}) conductivities measured at room temperature for the electric field processed ceramics.

E (V cm^{-1})	AGS (μm)	σ_{Bulk} (mS cm^{-1})	σ_{GB} (mS cm^{-1})
80	0.4	0.5	3.4×10^{-4}
100	0.8	0.5	5.9×10^{-4}

radiation approximation and are presented in the Supplementary Material Table S1. The temperature of the specimens also increases with E, which might justify the increase in grain size.

It has been shown that there exists a "safe" region of electrical parameters where the samples experience uniform flash sintering. By increasing field strength beyond "safe values" the ceramics display a non-uniform microstructure due to localization of the current flow [31]. Here, using $E \leq 120\,V\ cm^{-1}$ sintering was found to be uniform. However, for $E = 150\,V\ cm^{-1}$ the uniformity in mi-

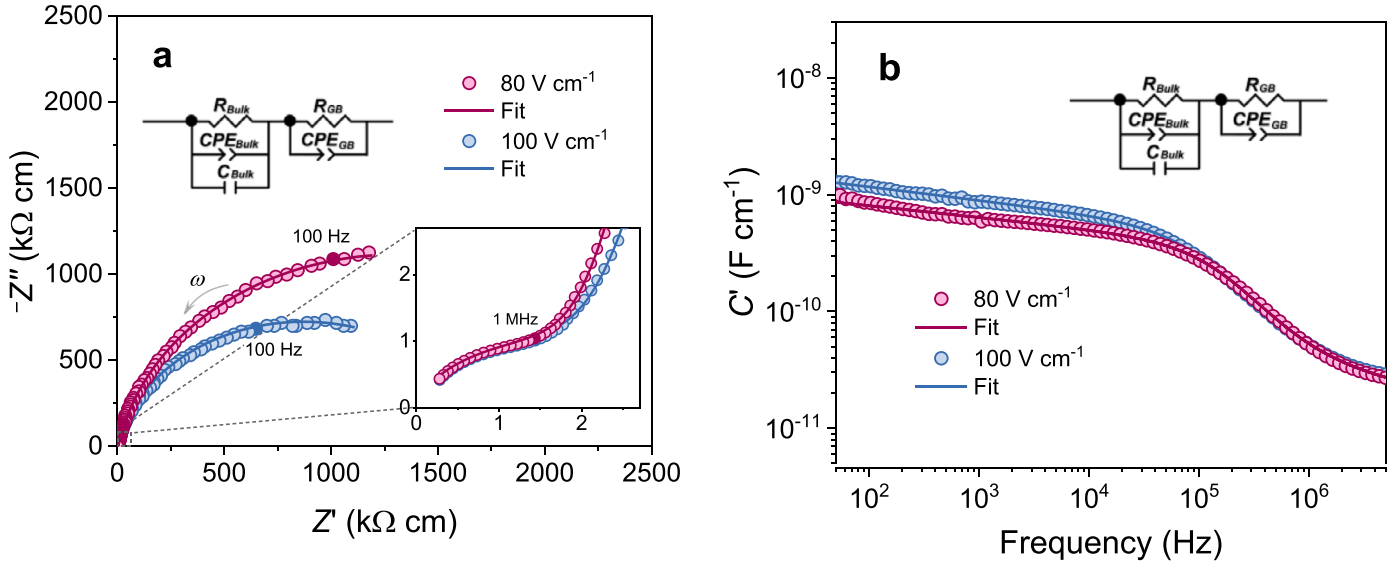

Fig. 4. (a) Impedance complex plane plots and (b) *C'* spectroscopic plots measured at room temperature for ceramics processed with different electric fields. The inset in (a) is a magnification of the data at high frequencies.

crostructure was lower, indicating the transition to a "non-safe" region. These results are presented in the Supplementary Material Figure S4.

The electrical properties of the specimens flashed at 80 and 100 V cm^{-1} were characterized by impedance spectroscopy. Pt paste was applied to the polished surfaces of the ceramics, and impedance data were recorded with a 4192A LF impedance analyzer (Hewlett Packard, Tokyo, Japan) in the frequency range of 50 Hz to 50 MHz with an applied potential of 100 mV.

The Nyquist plots of complex impedance $Z^* = Z' + iZ''$, corrected by sample geometry, are given in Fig. 4a. Two semi-circular arcs are shown, one at high and the other one at low frequencies. The spectroscopic plots of capacitance *C'* are given in Fig. 4b, where it is possible to observe a dielectric dispersion of almost two orders of magnitude between two plateau-like behaviors. The low frequency plateau ($\sim 10^{-11}$ F cm^{-1}) is ascribed to the *bulk* response, while the high-capacitance plateau ($\sim 10^{-9}$ F cm^{-1}) is interpreted as a grain boundary (GB) contribution [32]. Therefore, in the complex impedance plots the high frequency arc corresponds to the bulk response, and the low frequency to the GBs. The equivalent circuit adopted to fit the data, using the software ZView, is also given in Fig. 4. The good quality of the fit over the entire frequency range supports the model validity.

The bulk (σ_{Bulk}) as well as the GB (σ_{GB}) conductivities of these ceramics are included in Table 1. $\sigma_{Bulk} = 0.5$ mS cm^{-1} is in agreement with that obtained for $Li_{0.5}La_{0.5}TiO_3$ in previous studies [17].

Assuming a brick-layer model reduced to a series-layer model for describing grains and grain boundaries in electroceramics [33], the relationships between macroscopic and specific conductivities may be written as follows:

$$\sigma_{Bulk} \cong \sigma_{Bulk}^{sp}, \quad (1)$$

$$\sigma_{GB} \cong \sigma_{GB}^{sp} \frac{d}{\delta_{GB}}, \quad (2)$$

where "sp" refers to the specific or intrinsic values, *d* stands for the AGS and δ_{GB} represents the grain-boundary thickness. For these relations, the approximation $d >> \delta_{GB}$ was used. Therefore, from Eqs. (1) and (2), if the intrinsic conductivities of the ceramics do not change, consistent with the fact that the crystalline structure was found to be similar for both specimens, only the grain boundaries are expected to show a macroscopic conductivity dependent on the grain size. Indeed, by increasing the field from 80 to 100 V cm^{-1}, the same value of bulk conductivity was found and σ_{GB} increased in agreement with the increase in AGS. The low value of grain boundary conductivity on LLTO is known to hinder the Li-ion transfer. This is one of the obstacles to be overcome for materializing LLTO ceramics as electrolyte in solid state batteries [17].

Summarizing, the field-induced production of single-phase and highly dense LLTO ceramics in a single experiment was investigated, *i.e.*, with no need of a prior, separate, calcination step. Although green samples from the amorphous precursor yielded LLTO upon heating to 1150 °C, sintering was minimal. This is reasonable since the driving force for sintering is small (usually of the order of 100 J mol^{-1}) when compared to that of chemical reactions (of the order of kJ mol^{-1}) [34]. Therefore, it is expected that phase transformation takes place before sintering. Because of this, processing of ceramics normally involves several steps, including calcination at a relatively low temperature for synthesis of the end-product powder, then sintering at a high temperature for densification. In contrast, by applying an electric field, we achieved synthesis plus sintering of LLTO in a single-step experiment. The field-assisted processed ceramics presented a high bulk conductivity of 0.5 mS cm^{-1}, regardless of the magnitude of field applied during the processing. On the other hand, microstructural characteristics and grain boundary conductivity showed a dependence on the field strength used during the sintering. The simplicity of the procedure presented here and the rapid processing of single-phased, near fully-dense ceramics at low furnace temperatures opens new directions regarding the processing of complex oxides. Furthermore, the use of a chemical synthesis may facilitate doping of these oxides with different elements.

Acknowledgments

This work was supported by the São Paulo Research Foundation (FAPESP) [grant number 2018/19370–6]; the Coordination of Improvement of Higher Education Personnel (CAPES); the Army Research Office (ARO) [grant number W911NF-16-1-0200], under the direction of Dr. Michael Bakas; and the Office of Science of the Department of Energy [grant number DE-AC02-98CH10886]. This study used the 28ID-2 XPD beamline of the National Synchrotron Light Source II, a U.S. DOE Office of Science User Facility operated for the DOE Office of Science by Brookhaven National Laboratory

under Contract No. DE-SC0012704. The authors also wish to thank professor Don L. Williamson at Colorado School of Mines for the instrument and assistance to perform X-ray diffraction measurements during laboratory experiments.

Supplementary material

Supplementary material associated with this article can be found, in the online version, at doi:10.1016/j.scriptamat.2019.09.037.

References

[1] S.K. Jha, J.M. Lebrun, R. Raj, J. Eur. Ceram. Soc. 36 (2016) 733–739.
[2] D. Kok, D. Yadav, E. Sortino, S.J. McCormack, K.P. Tseng, W.M. Kriven, R. Raj, M.L. Mecartney, J. Am. Ceram. Soc. 102 (2019) 644–653.
[3] B. Yoon, D. Yadav, S. Ghose, R. Raj, J. Am. Ceram. Soc. 102 (2019) 2294–2303.
[4] B. Yoon, D. Yadav, S. Ghose, P. Sarin, R. Raj, J. Am. Ceram. Soc. 102 (2019) 3110–3116.
[5] H. Zhang, Y. Wang, J. Liu, X. Xu, L. Chen, D. Liu, Ceram. Int. 45 (2019) 13551–13555.
[6] E. Gil-González, A. Perejón, P.E. Sánchez-Jiménez, M.J. Sayagués, R. Raj, L.A. Pérez-Maqueda, J. Mater. Chem. A. 6 (2018) 5356–5366.
[7] V. Avila, R. Raj, J. Am. Ceram. Soc. 102 (2019) 6443–6448.
[8] L.M. Jesus, R.S. Silva, J.C. M'Peko, J. Adv. Ceram. 8 (2019) 265–277.
[9] L.M. Jesus, R.S. Silva, R. Raj, J.C. M'Peko, RSC Adv 6 (2016) 107208–107213.
[10] Y. Deng, S.J. Shang, A. Mei, Y.H. Lin, L.Y. Liu, C.W. Nan, J. Alloys Compd. 472 (2009) 456–460.
[11] H.X. Geng, A. Mei, C. Dong, Y.H. Lin, C.W. Nan, J. Alloys Compd. 481 (2009) 555–558.
[12] C.R. Milian Pila, T.M. Otero, E. Pérez Cappe, O.L. Alves, P. Aranda, M.A. Frutis, Y.M. Laffita, Ceram. Int. 40 (2014) 249–256.
[13] A. Varez, M.T. Fernández-Díaz, J.A. Alonso, J. Sanz, Chem. Mater. 17 (2005) 2404–2412.
[14] M. Chen, C. Huang, Y. Li, S. Jiang, P. Zeng, G. Chen, H. Shu, H. Liu, Z. Li, X. Wang, J. Mater. Chem. A. 7 (2019) 10293–10302.
[15] Y.R. Zhu, T.F. Yi, X.Y. Li, Y. Xie, S. Luo, Mater. Lett. 239 (2019) 56–58.
[16] J. Ibarra, A. Várez, C. León, J. Santamarıá, L.M. Torres-Martıńez, J. Sanz, Solid State Ion. 134 (2000) 219–228.
[17] Y. Sun, P. Guan, Y. Liu, H. Xu, S. Li, D. Chu, Crit. Rev. Solid State Mater. Sci. 44 (2018) 265–282.
[18] S. Stramare, V. Thangadurai, W. Weppner, Chem. Mater. 15 (2003) 3974–3990.
[19] A. Belous, O. Yanchevskiy, O. V'Yunov, O. Bohnke, C. Bohnke, F. Le Berre, J.L. Fourquet, Chem. Mater. 16 (2004) 407–417.
[20] M. Sommariva, M. Catti, Chem. Mater. 18 (2006) 2411–2417.
[21] A. Várez, J. Ibarra, A. Rivera, C. León, J. Santamaría, M.A. Laguna, M.L. Sanjuán, J. Sanz, Chem. Mater. 15 (2003) 225–232.
[22] R. Raj, J. Am. Ceram. Soc. 99 (2016) 3226–3232.
[23] B. Yoon, D. Yadav, R. Raj, E. Sortino, S. Ghose, P. Sarin, D. Shoemaker, J. Am. Ceram. Soc. 101 (2018) 1811–1817.
[24] X. Shi, S. Ghose, E. Dooryhee, J. Synchrotron Radiat. 20 (2013) 234–242.
[25] T.N.H. Le, M. Roffat, Q.N. Pham, S. Kodjikian, O. Bohnke, C. Bohnke, J. Sol-Gel Sci. Technol. 46 (2008) 137–145.
[26] W. Liu, K.M. Liang, Y.K. Zheng, S.R. Gu, H. Chen, J. Phys. D: Appl. Phys. 30 (1997) 3366–3370.
[27] J.R. Carvajal, in: Proceedings of the Satellite Meeting on Powder Diffraction of the XV Congress of the IUCr, France, 1990.
[28] Y. Harada, T. Ishigaki, H. Kawai, J. Kuwano, Solid State Ion 108 (1998) 407–413.
[29] H. Geng, A. Mei, Y. Lin, C. Nan, Mater. Sci. Eng., B. 164 (2009) 91–95.
[30] S.K. Jha, R. Raj, J. Am. Ceram. Soc. 97 (2014) 527–534.
[31] J.C. M'Peko, J.S.C. Francis, R. Raj, J. Eur. Ceram. Soc. 34 (2014) 3655–3660.
[32] J.T.S. Irvine, D.C. Sinclair, A.R. West, Adv. Mater. 2 (1990) 132–138.
[33] E. Barsoukov, J.R. Macdonald, Impedance Spectroscopy: Theory, Experiment, and Applications, 2nd ed., A John Wiley & Sons, Inc., New Jersey, 2005.
[34] M. Barsoum, Fundamentals of Ceramics, 1st ed., Institute of Physics Publishing, London, 2003.